

Ultrafast and Fault-Tolerant Quantum Communication across Long Distances

Sreraman Muralidharan¹, Jungsang Kim², Norbert Lütkenhaus³, Mikhail D. Lukin⁴, and Liang Jiang⁵

¹*Department of Electrical Engineering, Yale University, New Haven, CT 06511 USA*

²*Department of Electrical and Computer Engineering, Duke University, Durham, NC 27708 USA*

³*Institute of Quantum computing, University of Waterloo, N2L 3G1 Waterloo, Canada*

⁴*Department of Physics, Harvard University, Cambridge, MA 02138, USA and*

⁵*Department of Applied Physics, Yale University, New Haven, CT 06511 USA*

(Dated: September 11, 2022)

Quantum repeaters (QRs) provide a way of enabling long distance quantum communication by establishing entangled qubits between remote locations. In this Letter, we investigate a new approach to QRs in which quantum information can be faithfully transmitted via a noisy channel without the use of long distance teleportation, thus eliminating the need to establish remote entangled links. Our approach makes use of small encoding blocks to fault-tolerantly correct both operational and photon loss errors. We describe a way to optimize the resource requirement for these QRs with the aim of the generation of a secure key. Numerical calculations indicate that the number of quantum memory bits required for our scheme has favorable poly-logarithmic scaling with the distance across which the communication is desired.

PACS numbers: 03.67.Dd, 03.67.Hk, 03.67.Pp.

Quantum communication across long distances (10^3 - 10^4 km) can significantly extend the applications of quantum information protocols such as quantum cryptography [1] and quantum secret sharing [2, 3] which can be used for the creation of a secure quantum internet [4]. Quantum communication can be carried out by first establishing a remote entangled pair between the sender and the receiver and using teleportation to transmit information faithfully. However, there are two main challenges that have to be overcome. First, fiber attenuation during transmission leads to an exponential decrease in entangled pair generation rate. Second, several operational errors such as channel errors, gate errors, measurement errors and quantum memory errors severely degrade the quality of entanglement used for secure key generation. In addition, quantum states cannot be amplified or duplicated deterministically in contrast to classical information [5]. Establishing quantum repeater (QR) stations based on entanglement distribution is the only currently known approach to long-distance quantum communication using conventional optical fibers without exponential penalty in time and resources.

A number of schemes have been proposed for long distance quantum communication using QRs [6–12], most of which could be broadly classified into three classes. The first class of QRs [6–9] reduces the exponential scaling of fiber loss to polynomial scaling by introducing intermediate QR nodes. However, this scheme for long distance quantum communication is relatively slow [13], even after optimization [14], limited by the time associated with two-way classical communication between remote stations required for the entanglement purification process needed to correct operational errors [15]. In contrast, the second class of QRs introduce quantum encoding and classical error correction to replace the entanglement purification with classical error correc-

tion, handling all operational errors [10, 16]. As a consequence, the entanglement generation rate further improves from $O(\text{poly}(L_{tot}))$ to $O(\text{poly}(\log(L_{tot})))$ where L_{tot} is the total distance of communication. Recently, the approach to the third type of QRs was proposed, which uses quantum encoding to deterministically correct photon losses [11, 12]. By entirely eliminating two-way classical communication between *all* repeater stations, the third class of QRs promise extremely high key generation rates that can be close to classical communication rates, limited only by the speed of local operations.

Besides high key generation rate, it is very important to consider the resource requirement and fault-tolerant implementation for this type of QRs. In the fault-tolerant surface-code proposal by Fowler *et. al.* [11], the resource for each station was estimated to scale logarithmically with the distance, while the exact resource overhead was found to be sensitive to the parameters for various imperfections. The proposal by Munro *et. al.* [12] focused on the correction of photon loss errors using quantum parity code (QPC) [17], but did not consider fault-tolerance, as perfect gate operations were assumed in their analysis. In this Letter, we propose a fault-tolerant architecture for third class of QRs, where a teleportation-based error correction (TEC) protocol [18, 19] is employed *within* each repeater station to correct both operational and photon loss errors using Calderbank-Shor-Steane (CSS) encoding. We quantitatively investigate the optimum resource requirements using a *cost function* and optimize it for different repeater parameters. A schematic view of the proposed architecture of the third class of QRs is presented in Fig. 1.

Fault-tolerant architecture. Analogous to fault-tolerant quantum computers [20], fault-tolerant QRs should reliably relay quantum information from one repeater station to another in the presence of various

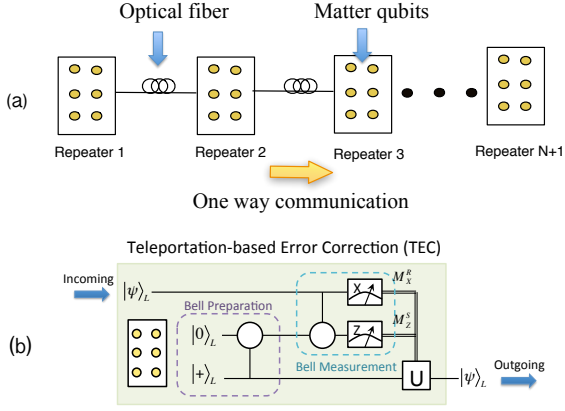


FIG. 1: (color online). (a) A schematic view of the third class of QRs showing individual matter qubits in the repeater stations connected by an optical fiber. The quantum state is encoded into an error correcting code with photonic qubits, which are multiplexed and transmitted through the optical fiber to the neighboring repeater station. The quantum state of photonic qubits is transferred to the matter qubits and error correction is performed. After the error correction procedure, the quantum state of the matter qubits is transferred to photonic qubits and transmitted to the next repeater station. This procedure is carried out until the information reaches the receiver. (b) The TEC procedure consists of Bell state preparation and Bell measurement at the encoded level. Each line in the circuit represents an encoding block and the CNOT gate has a transversal implementation for CSS codes. This TEC scheme can be potentially implemented in a cavity QED system [21, 22].

imperfections. Unlike quantum computers, QRs do not require a universal gate set and it is sufficient to have CNOT gates and state initialization/measurement associated with the complimentary basis of $\{|0\rangle, |1\rangle\}$ and $\{|+\rangle, |-\rangle\}$. However, QRs are confronted by an important challenge from transmission loss, which is less severe in most models of quantum computation. To design fault-tolerant third class of QRs, we consider the CSS codes for their fault-tolerant properties [20], in particular the compatibility with the TEC protocol that can efficiently correct not only operational errors, but also photon loss errors [18, 19]. The (n, m) -QPC [17] is a class of CSS codes with encoded qubits $|0\rangle_L = \frac{1}{\sqrt{2}}(|+\rangle_L + |-\rangle_L)$ and $|1\rangle_L = \frac{1}{\sqrt{2}}(|+\rangle_L - |-\rangle_L)$, where $|\pm\rangle_L$ are given by

$$\begin{aligned} |+\rangle_L &= \frac{1}{2^{n/2}} (|00\dots 0\rangle_{12\dots m} + |11\dots 1\rangle_{12\dots m})^{\otimes n} \\ |-\rangle_L &= \frac{1}{2^{n/2}} (|00\dots 0\rangle_{12\dots m} - |11\dots 1\rangle_{12\dots m})^{\otimes n}. \end{aligned} \quad (1)$$

The (n, m) -QPC consists of n sub-blocks, and each sub-block has m physical qubits. First, we define the Pauli operators, $X_{i,j}, Y_{i,j}, Z_{i,j}$ associated the (i, j) -th qubit, where $i = 1, \dots, n$ is the row (sub-block) label and $j = 1, \dots, m$ is the column label for the qubit. There is

one logical qubit encoded in the (n, m) -QPC, with logical operators $\tilde{Z} \equiv \prod_{i=1}^n Z_{i,j}$ and $\tilde{X} \equiv \prod_{j=1}^m X_{i,j}$, where we may choose any $j = 1, \dots, m$ for \tilde{Z} and any $i = 1, \dots, n$ for \tilde{X} [20]. The encoded states $\{|0\rangle_L, |1\rangle_L, |+\rangle_L, |-\rangle_L\}$ can be prepared fault-tolerantly with independent errors acting on individual physical qubits [22–24]. The encoded state is transmitted via an optical fiber to the neighboring repeater station followed by error correction and transmission to the next repeater station (Fig. 1).

Suppose that each transmitted physical qubit can reach the next QR station with probability η , meanwhile suffering from depolarization errors. We apply TEC [18, 19] to correct both photon loss and depolarization errors. The TEC procedure consists of Bell state preparation and Bell measurement at the encoded level (Fig. 1 (b)), and both operations can be achieved fault-tolerantly without propagating errors within each encoding block [20]. The Bell measurement of two encoded blocks (received block R and local block S) can be achieved by an encoded CNOT gate followed by measurement of logical operators \tilde{X}^R and \tilde{Z}^S . More specifically, it consists of nm pair-wise CNOT gates between $R_{i,j}$ and $S_{i,j}$, followed by $2nm$ individual qubit measurements. Besides erasure errors, TEC can also correct various other imperfections of fiber depolarization, encoding blocks, CNOT gates and qubit measurements, which can be captured by an effective error probability ε acting on single qubit for our fault tolerant circuit designs [22].

In the presence of photon loss errors, each measurement may have three possible outcomes $\{+1, -1, 0\}$. Each qubit $R_{i,j}$ in the R block is measured in the X basis with outcome $X_{i,j}^R$ taking value $+1$ for qubit state $|+\rangle$, -1 for qubit state $|-\rangle$, and 0 if the qubit is erased due to transmission loss. Similarly, each qubit $S_{i,j}$ from the S block is measured in the Z basis with outcome $Z_{i,j}^S$ taking value $+1$ for qubit state $|0\rangle$, -1 for qubit $|1\rangle$, and 0 if the corresponding qubit in the R -block ($R_{i,j}$) is erased. The logical measurement outcomes depend on individual qubit measurement outcomes

$$\tilde{M}_X^R = \text{sign} \left[\sum_{i=1}^n \left(\prod_{j=1}^m X_{i,j}^R \right) \right], \quad \tilde{M}_Z^S = \prod_{i=1}^n \left(\text{sign} \left[\sum_{j=1}^m Z_{i,j}^S \right] \right),$$

with three possible values $\{+1, -1, 0\}$. Here $\text{sign}[\sum \dots]$ is associated with majority voting between $\{\pm 1\}$, and $\prod \dots$ is associated with the product of trinary outcomes. Ideally, in the absence of errors, the outcomes should be $\tilde{M}_X^R = \tilde{X}^R$ and $\tilde{M}_Z^S = \tilde{Z}^S$, which determine the Pauli frame [18, 19] of the encoded block after teleportation. In the presence of errors, however, the outcomes become $\tilde{M}_X^R = \alpha \tilde{X}^R$ and $\tilde{M}_Z^S = \beta \tilde{Z}^S$, with $\alpha, \beta = +1$ for correct measurement, -1 for incorrect measurement, and 0 for heralded failure of measurement. We obtain the probability distribution (see Fig. 2a) [22] $p_{\alpha,\beta} \equiv \Pr \left[\tilde{M}_X^R = \alpha \tilde{X}^R, \tilde{M}_Z^S = \beta \tilde{Z}^S \right]$, which can be used to evaluate the QR performance.

Quantum bit error rate and success probability We use the probability distribution to compute the success probability and quantum bit error rate (QBER) that characterizes the QR. Since the encoded qubit passes through N repeater stations, there are N pairs of measurement outcomes (\tilde{M}_X and \tilde{M}_Z). The success probability with no heralded failure of measurements is

$$P_{succ} = (p_{1,1} + p_{1,-1} + p_{-1,1} + p_{-1,-1})^N. \quad (2)$$

Given that all measurement outcomes have no heralded failure, there might be an odd number of incorrect measurements of \tilde{M}_X (or \tilde{M}_Z), which induces an error if the receiver decodes the information by measuring \tilde{X} (or \tilde{Z}) of the received block. We define the QBER at the encoded level of the QR as the ratio of the probability of having an odd number of incorrect measurements of \tilde{M}_X (or \tilde{M}_Z) to the probability of having no heralded failure. The QBER for \tilde{X} (or \tilde{Z}) measurement by the receiver is

$$Q_{(X/Z)} = \frac{1}{2} \left[1 - \frac{(p_{1,1} \pm p_{1,-1} \mp p_{-1,1} - p_{-1,-1})}{p_{1,1} + p_{1,-1} + p_{-1,1} + p_{-1,-1}} \right]^N. \quad (3)$$

Key generation rate. For our QR, the raw key generation rate is $1/t_0$, where t_0 is the time taken for TEC. For simplicity, we may use t_0 as a time unit in our analysis. The raw keys can be converted to secure keys through classical communication protocols involving error correction and privacy amplification [1]. Due to finite success probability and non-vanishing QBER, the asymptotic secure key generation rate is given by [25, 26]

$$R = \max \left[\frac{1}{t_0} P_{succ} (1 - 2h(Q)), 0 \right], \quad (4)$$

where $Q = \frac{(Q_X + Q_Z)}{2}$ and $h(Q) = -Q \log_2(Q) - (1 - Q) \log_2(1 - Q)$ is the binary entropy function. In Fig. 2, we show that R can approach $1/t_0$ for reasonable encoding size ($n \times m$) with an appropriate repeater spacing (L_0), because it is possible to achieve high P_{succ} and low Q . The range of (n, m) that yields a high key generation rate varies with L_0 and the total distance of communication $L_{tot} (= N \times L_0)$. Hence, we need to optimize the repeater parameters, including the size of encoding block, repeater spacing, and secure key generation rate.

For each secret bit generated by the QR, we should consider the cost of both time and qubit resources [27]: (1) the average time to generate a secret bit is $1/R$, and (2) the total number of memory qubits needed for the QR scheme is $2nm \times \frac{L_{tot}}{L_0}$ [45]. We introduce the *cost function*, C to be the product of these two factors $\frac{2nm}{R} \times \frac{L_{tot}}{L_0}$, in units of [qubits $\cdot t_0$ /sbit]. Here the rate R implicitly depends on the control parameters of $\{n, m, L_0\}$. For given L_{tot} , we can achieve the minimum cost:

$$C(L_{tot}) \equiv \min_{n, m, L_0} \frac{2nm}{R} \times \frac{L_{tot}}{L_0}, \quad (5)$$

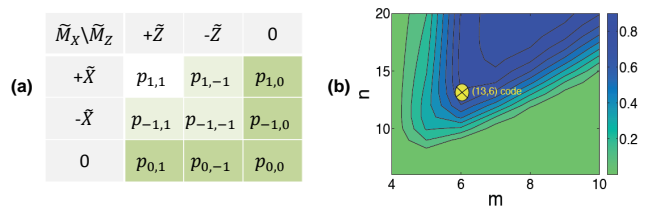


FIG. 2: (color online). (a) Distribution of possible measurement outcomes. Measurement outcomes in the lighter area ($p_{1,-1}$, $p_{-1,1}$, $p_{-1,-1}$) are logical errors, and outcomes in the darker area ($p_{\alpha,0}$ and $p_{0,\beta}$) lead to heralded failure. (b) Contour plot for the key generation rate $R(n, m)$ (with $t_0 = 1$) across a total distance $L_{tot} = 10,000$ km with repeater spacing $L_0 = 1.5$ km and $\varepsilon = 10^{-3}$. The optimized choice of encoding with minimum cost [see Eq. (5)] is a (13,6) code.

among all possible choices of (n, m) -QPC and repeater spacing L_0 . We assume the following imperfections as we search for the optimal scheme: (1) depolarization error with probability ε , and (2) finite photon transmission with probability $\eta = (1 - p_c)e^{-L_0/L_{att}}$ due to fiber attenuation ($L_{att} = 20$ km) and coupling loss (p_c).

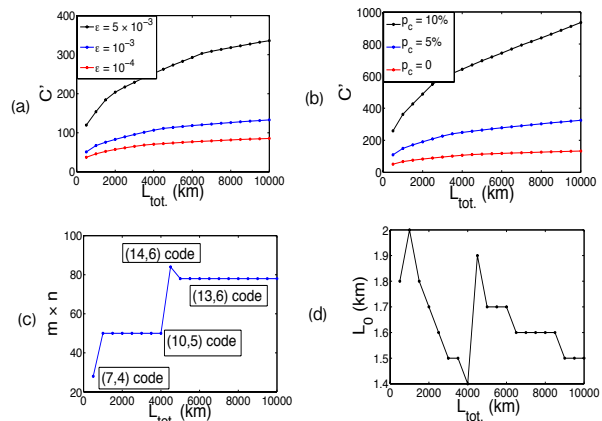


FIG. 3: (color online). (a) Cost coefficient $C'(L_{tot})$ for different operational errors ε with zero coupling loss $p_c = 0$, (b) cost coefficient $C'(L_{tot})$ for varying p_c with fixed $\varepsilon = 10^{-3}$, (c,d) optimized encoded block size and repeater spacing for $\varepsilon = 10^{-3}$ and $p_c = 0$.

Numerical search for optimized strategy. We search for optimized choices of $\{n, m, L_0\}$ for different values of L_{tot} with fixed imperfection parameters of $\{\varepsilon, p_c\}$. We run a numerical search for L_0 in the range 0.1 km $< L_0 < 4$ km and for different number of qubits in the range $2 < (n, m) < 50$ to obtain $C(L_{tot})$, which should increase at least linearly with L_{tot} . In Fig. 3, we show the variation of *cost coefficient* ($C' = C/L_{tot}$) with L_{tot} , to illustrate the additional overhead associated with L_{tot} . The cost coefficient can be interpreted as the resource overhead (qubits $\times t_0$) for creating one secret bit over 1 km (with target distance L_{tot}).

For imperfection parameters of $\epsilon = 10^{-3}$ and $p_c = 0$, the algorithm picks only four different codes up to $L_{tot} = 10,000$ km. When the code chosen by the algorithm changes (for example at 4500 km in Fig. 3), the product of L_0 and R also jumps to an appropriate higher value, so that the cost coefficient varies continuously with L_{tot} . In the presence of coupling loss $p_c < 10\%$, the optimized values of L_0 is within the range $1.4 \sim 2$ km (Fig. 3) with total loss errors up to 20%; $R \cdot t_0$ is high (0.6 – 0.85) because of the favorable QBER associated with the chosen codes.

The optimized cost coefficient for different operational error probabilities is shown in Fig. 3. When ϵ decreases below 10^{-3} , the cost coefficient is dominated by photon loss errors rather than operational errors, and does not decrease by a significant amount as ϵ decreases further. In a realistic scenario, photons are lost due to finite coupling losses besides fiber attenuation. In Fig. 3, we show that the QR scheme can tolerate coupling losses up to 10% for a reasonable overhead in the number of qubits. Numerical calculations indicate that the cost coefficient increases by $O(\text{poly}(\log(L_{tot})))$ [22]. Table I provide an estimate of the resource requirements of our code under different scenarios.

Experimental consideration. To implement the QR scheme, it is crucial to fulfill the following two experimental requirements: (1) The coupling loss should be sufficient low ($p_c \leq 10\%$) for our QR scheme. In fact, one should have $(1 - \eta) < 50\%$ for one-way QR schemes to work as required by the quantum no-cloning theorem. Recently, there are significant developments of fiber-to-chip grating couplers with coupling efficiency of -1.6 dB (i.e., $p_c \approx 30\%$) [28], which makes the low coupling loss feasible. (2) Quantum repeater station should have hundreds of qubits with high fidelity operations. For ion trap systems, single qubit gate error probability of 2×10^{-5} [29], two-qubit gate error probability of 0.007 [30], and measurement error probability of 10^{-4} [31, 32] have been demonstrated. There are also promising developments in micro-fabricated ion traps for coherent control of hundreds of ion qubits [33]. In addition to these two requirements, efficient downconversion to telecom wavelength (e.g., [34] achieving 80% internal conversion efficiency) can be very helpful to minimize fiber attenuation. [46]

The techniques of time and wavelength-division-multiplexing will enable us to transmit all the photons through a single optical fiber. The operation of TEC can be achieved with cavity QED systems [21, 22]. The performance of the QR scheme introduced here depends crucially on the range of input parameters (ϵ, p_c, t_0). The key generation rate R depends on the TEC time of t_0 . Since it is possible to have sub-nanosecond quantum gates [35, 36] with trapped ions, the TEC time will be mostly limited by the relatively slow measurement ($10 \sim 100\mu s$) [37] due to finite photon scattering rate and collection efficiency, which can be significantly im-

p_c	ϵ	$L_{tot} = 1000$ km				$L_{tot} = 10000$ km			
		m	n	L_0 (km)	$R \cdot t_0$	m	n	L_0 (km)	$R \cdot t_0$
0%	10^{-4}	4	7	1.7	0.72	5	9	1.3	0.80
0%	10^{-3}	5	10	2.0	0.74	6	13	1.5	0.78
10%	10^{-4}	6	21	1.6	0.60	7	28	1.0	0.57
10%	10^{-3}	7	31	1.8	0.67	8	41	1.2	0.59

TABLE I: Optimized resource requirements for our fault tolerant QR scheme with (n, m) -QPC encoding for different coupling losses p_c and operational error ϵ .

proved by enhancing the ion-cavity coupling strength. For instance, if the TEC time is improved to $t_0 = 1 \mu s$, a secure key generation rate approaching MHz can be achieved over 10,000 km. The ion-cavity coupling loss can be suppressed by the Purcell effect in ion-cavity systems, and our scheme can tolerate up to 10% coupling loss without significant increase of the cost coefficient.

Besides trapped ions, NV centers [38, 39], quantum dots [40, 41], and Rydberg atoms [42, 43] are also promising systems for quantum repeater implementations. Furthermore, with the advance of coherent conversion between optical and microwave photons [44], superconducting qubits may become an attractive candidate to realize our scheme as they can achieve both ultrafast quantum gates and high coupling efficiency.

Summary and Outlook. We have presented a new QR scheme belonging to the third class of QRs which considers both fault tolerance and small encoding blocks for ultrafast quantum communication over long distances. In comparison with the first and second classes of QR schemes, our QR scheme uses TEC within each QR station to correct both photon loss and operation errors. In particular, our QR scheme can tolerate finite coupling loss ($p_c \lesssim 10\%$) and achieve fault-tolerant operation with approximately hundreds of qubits per repeater station. This enables improved key generation rate that is limited only by local gate operations. Our scheme requires smaller QR spacing compared to the previous classes of QRs and consequently the number of QR stations is higher by roughly an order of magnitude. But it is important to note that the key generation rate increases by more than three orders of magnitude, by eliminating the communication time between the repeater stations. In addition, we have introduced a cost function to optimize the control parameters of our QR scheme, which can potentially be used as a criterion to compare all three classes of QRs as well as to search for more efficient quantum error correcting codes for quantum communication.

Acknowledgements This work was supported by DARPA Quiness grant, NBRPC (973 program), and the Alfred P. Sloan Foundation. We thank Austin Fowler, Steven Girvin, Archana Kamal, Chris Monroe, Bill Munro, David Poulin and Hong Tang for discussions.

-
- [1] N. Gisin, G. Ribordy, W. Tittel, and H. Zbinden, *Rev. Mod. Phys.* **74**, 145 (2002).
- [2] R. Cleve, D. Gottesman, and H. K. Lo, *Phys. Rev. Lett.* **83**, 648 (1999).
- [3] M. Hillery, V. Buzek, and A. Berthiaume, *Phys. Rev. A* **59**, 1829 (1999).
- [4] H. J. Kimble, *Nature* **453**, 1023 (2008).
- [5] W. K. Wootters and W. H. Zurek, *Nature* **299**, 802 (1982).
- [6] H. J. Briegel, W. Dür, J. I. Cirac, and P. Zoller, *Phys. Rev. Lett.* **81**, 5932 (1998).
- [7] W. Dür, H. J. Briegel, J. I. Cirac, and P. Zoller, *Phys. Rev. A* **59**, 169 (1999).
- [8] L. M. Duan, M. D. Lukin, J. I. Cirac, and P. Zoller, *Nature* **414**, 413 (2001).
- [9] P. van Loock, T. D. Ladd, K. Sanaka, F. Yamaguchi, K. Nemoto, W. J. Munro, and Y. Yamamoto, *Phys. Rev. Lett.* **96**, 240501 (2006).
- [10] L. Jiang, J. M. Taylor, K. Nemoto, W. J. Munro, R. Van Meter, and M. D. Lukin, *Phys. Rev. A* **79**, 032325 (2009).
- [11] A. G. Fowler, D. S. Wang, C. D. Hill, T. D. Ladd, R. Van Meter, and L. C. L. Hollenberg, *Phys. Rev. Lett.* **104**, 180503 (2010).
- [12] W. J. Munro, A. M. Stephens, S. J. Devitt, K. A. Harrison, and K. Nemoto, *Nat. Phot.* **6**, 777 (2012) (Also see quantph/1306.4137).
- [13] N. Sangouard, C. Simon, H. de Riedmatten, and N. Gisin, *Rev. Mod. Phys.* **83**, 33 (2011).
- [14] L. Jiang, J. M. Taylor, N. Khaneja, and M. D. Lukin, *Proc. Natl. Acad. Sci. U.S.A* **104**, 17291 (2007).
- [15] C. H. Bennett, G. Brassard, S. Popescu, B. Schumacher, J. A. Smolin, and W. K. Wootters, *Phys. Rev. Lett.* **76**, 722 (1996).
- [16] W. J. Munro, K. A. Harrison, A. M. Stephens, S. J. Devitt, and K. Nemoto, *Nat. Phot.* **4**, 792 (2010).
- [17] T. C. Ralph, A. J. F. Hayes, and A. Gilchrist, *Phys. Rev. Lett.* **95**, 100501 (2005).
- [18] E. Knill *Nature* **434**, 39 (2005) (Also see quantph/0410199v2).
- [19] E. Knill, R. Laflamme, and G. J. Milburn, *Nature* **409**, 46 (2001).
- [20] M. A. Nielsen and I. L. Chuang, *Quantum Computation and Quantum Information* (Cambridge Univ. Press, 2002).
- [21] L. M. Duan and H. J. Kimble, *Phys. Rev. Lett.* **92**, 127902 (2004).
- [22] See Supplemental material for a detailed description of the error correction scheme, implementation of TEC, in depth analytical treatment of error correction, fault tolerant preparation of the encoded Bell pair, details of the optimization algorithm and the scaling of the cost function with respect to total distance of communication.
- [23] A. J. F. Hayes, H. L. Haselgrove, A. Gilchrist, and T. C. Ralph, *Phys. Rev. A* **82**, 022323 (2010).
- [24] P. Brooks and J. Preskill, *Phys. Rev. A* **87**, 032310 (2013).
- [25] P. W. Shor and J. Preskill, *Phys. Rev. Lett.* **85**, 441 (2000).
- [26] V. Scarani, H. B. Pasquinucci, N. J. Cerf, M. Dušek, N. Lütkenhaus, and M. Peev, *Rev. Mod. Phys.* **81**, 1301 (2009).
- [27] R. Alléaume, F. Roueff, E. Diamanti, and N. Lütkenhaus, *New Jour. Phys.* **11**, 075002 (2009).
- [28] D. Vermeulen, S. Selvaraja, P. Verheyen, G. Lepage, W. Bogaerts, P. Absil, D. Van Thourhout, and G. Roelkens, *Optics Express* **18**, 18278 (2010).
- [29] K. R. Brown, A. C. Wilson, Y. Colombe, C. Ospelkaus, A. M. Meier, E. Knill, D. Leibfried, and D. J. Wineland, *Phys. Rev. A* **84**, 030303 (2011).
- [30] J. Benhelm, G. Kirchmair, C. F. Roos, and R. Blatt, *Nat. Phys.* **4**, 463 (2008).
- [31] A. H. Myerson, D. J. Szwer, S. C. Webster, D. T. C. Allcock, M. J. Curtis, G. Imreh, J. A. Sherman, D. N. Stacey, A. M. Steane, and D. M. Lucas, *Phys. Rev. Lett.* **100**, 200502 (2008).
- [32] D. B. Hume, T. Rosenband, and D. J. Wineland, *Phys. Rev. Lett.* **99**, 120502 (2007).
- [33] C. Monroe and J. Kim, *Science* **339**, 1164 (2013).
- [34] J. S. Pelc, L. Yu, K. De Greve, P. L. McMahon, C. M. Natarajan, V. Esfandyarpour, S. Maier, C. Schneider, M. Kamp, S. Höfling, R. H. Hadfield, A. Forchel, Y. Yamamoto and M. M. Fejer, *Optics Express* **20**, 27510 (2012).
- [35] G. Romero, D. Ballester, Y. M. Wang, V. Scarani, and E. Solano, *Phys. Rev. Lett.* **108**, 120501 (2012).
- [36] W. C. Campbell, J. Mizrahi, Q. Quraishi, C. Senko, D. Hayes, D. Hucul, D. N. Matsukevich, P. Maunz, and C. Monroe, *Phys. Rev. Lett.* **105**, 090502 (2010).
- [37] R. Noek, G. Vrijsen, D. Gaultney, E. Mount, T. Kim, P. Maunz, and J. Kim, quantph/1304.3511
- [38] E. Togan, Y. Chu, A. S. Trifonov, L. Jiang, J. Maze, L. Childress, M. V. G. Dutt, A. S. Sørensen, P. R. Hemmer, A. S. Zibrov, and M. D. Lukin, *Nature (London)* **466**, 730 (2010).
- [39] H. Bernien, B. Hensen, W. Pfaff, G. Koolstra, M. S. Blok, L. Robledo, T. H. Taminiau, M. Markham, D. J. Twitchen, L. Childress, and R. Hanson, *Nature (London)* **497**, 86 (2012).
- [40] W. B. Gao, P. Fallahi, E. Togan, J. M. Sanchez, and A. Imamoglu, *Nature (London)* **491**, 426 (2012).
- [41] K. D. Greve, L. Yu, P. L. McMahon, J. S. Pelc, C. M. Natarajan, N. Y. Kim, E. Abe, S. Maier, C. Schneider, M. Kamp, S. Höfling, R. H. Hadfield, A. Forchel, M. M. Fejer, and Y. Yamamoto, *Nature (London)* **491**, 421 (2012).
- [42] T. Peyronel, O. Firstenberg, Q. Y. Liang, S. Hofferberth, A. V. Gorshkov, T. Pohl, M. D. Lukin, and V. Vuletić *Nature* **488**, 57 (2012).
- [43] Y. O. Dudin and A. Kuzmich, *Science* **336**, 887 (2012).
- [44] J. M. Taylor, A. S. Sørensen, C. M. Marcus, and E. S. Polzik, *Phys. Rev. Lett.* **107**, 273601 (2011).
- [45] Each repeater station needs $2mn$ memory qubits to store the encoded Bell pair. A small overhead (e.g. additional $\sim mn$ ancillary qubits) can enable fault-tolerant preparation of the encoded Bell pair. To fix ideas, we will use the number of memory qubits $2mn$ in our calculations.
- [46] However, our repeater scheme does not have to send photons at telecom wavelength, because the reduced attenuation length only leads to a linear overhead in the number of repeater stations (L_{tot}/L_{att}) and poly-log overhead in the number of qubits per station $poly(\log(L_{tot}/L_{att}))$, in contrast to the exponential overhead of direct quantum communication over the entire distance.

SUPPLEMENTAL MATERIAL

In the Supplemental material, we provide an introduction to the Quantum repeater (QR) scheme, a detailed description of error correction, implementation of teleportation based error correction (TEC) in a cavity-QED system, an in-depth analytical treatment of quantum error correction, fault tolerant preparation of the encoded Bell pair, details of the optimization algorithm and discuss the scaling of the cost function with respect to total distance of communication.

INTRODUCTION

The first two classes of QRs required the generation of heralded EPR pairs between neighboring repeater stations, and entanglement purification or quantum error correction steps to generate an EPR pair of high fidelity between distant repeater stations. If a photon is lost in the procedure, the heralded outcome will be a failure and the procedure will be repeated until it succeeds. Therefore, photon loss events do not have a major role to play in the success or the failure rates of the protocol. However, the heralded outcome requires two-way classical communication, which limits the key generation rate of the first two classes of QRs. In our new scheme for QRs, entanglement purification steps (in the first class of QRs) and the heralded entanglement generation steps (in the second class of QRs) are replaced by quantum error correction at individual repeater stations, eliminating the need to establish entangled links between any two repeater stations. Such a procedure makes use of one way classical communication which can be very fast and only limited by the speed of local operations. On the other hand, photon losses during the transmission of the encoded state may lead to failure events in the secret key generation. Hence, it is important that the error correction procedure at individual repeater stations can correct both loss and operational errors.

Keeping this in mind, we choose the Calderbank-Shor-Steane (CSS) encoding because they have properties of fault-tolerant state initialization and gate implementation. For instance, an encoded CNOT gate between the codewords can be achieved by simply applying transversal CNOT gates between the physical qubits. As we will see later, this is essential to perform a fault-tolerant quantum error correction at individual repeater stations.

DESCRIPTION OF THE ERROR CORRECTION SCHEME

When an encoded block of photons reaches a repeater station, missing photons are detected through a quantum non-destructive measurement and the remaining photons

are taken through a teleportation based error correction (TEC) protocol which is used to detect and correct both photon loss errors and operational errors. The TEC scheme makes use of an encoded Bell pair at every repeater station and an encoded CNOT gate followed by measurement of encoded X and Z operators. For all CSS codes, an encoded CNOT gate can be achieved through a CNOT gate between the k^{th} qubit of the first block and the k^{th} qubit of the second block for all k . The simplest illustration of the algorithm is shown in Fig. (4) where a (3,3)-QPC is used to correct loss of one photon in the absence of operational errors.

In a realistic scenario, we will also have operational errors due to gate errors, measurement errors, memory errors etc. As we will see, the TEC protocol is effective in protecting the qubits from both memory errors and operational errors. We use stabilizer formalism to understand how the majority voting process works in the presence of both these errors. Firstly, let's consider the presence of loss in determining the outcome of the X -measurement.

Recall that $\tilde{X} \equiv \prod_{j=1}^m X_{i,j}$ for $i = 1, \dots, n$ the presence of photon losses, As illustrated in Table. II with $(n, m) = (5, 4)$ encoding, we rearrange the encoding blocks such that the first $n' = 2$ sub-blocks (rows) contain missing qubits, while the remaining $n - n'$ sub-blocks are complete sub-blocks. All the qubits are measured in the \tilde{X} basis. The i -th complete sub-block can infer the \tilde{X} operator by computing $X_i^* \equiv \prod_{j=1}^m X_{i,j}$. The last step is to use majority voting among complete sub-blocks $\{X_i^*\}_{i=n'+1, n'+2, \dots, n}$ to obtain the true value of \tilde{X} . For codes with a larger number of qubits, the error

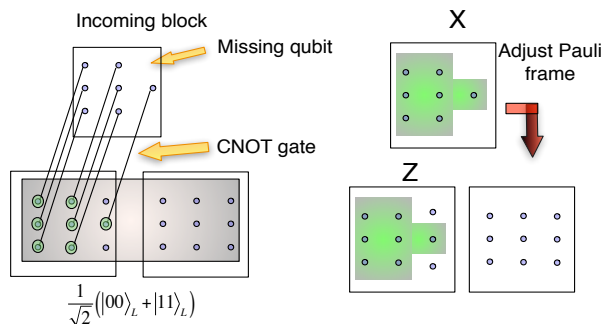


FIG. 4: (color online). An illustration of the TEC scheme using (3,3)-QPC to correct the loss of two photons. The photons at positions (1,3) and (3,3) are missing in the first block and consequently a CNOT gate is not applied between the first block and the second block at those positions. Subsequently, an encoded X and Z -measurements are carried out and the outcomes of the measurement are used to adjust the Pauli frame either at the same repeater station or transmitted to the receiver station and the Pauli frame is adjusted. The grey shading represents entanglement before the CNOT gate is applied and the green shade represents a measurement.

$i \setminus j$	1	2	3	4	$X_i^* \equiv \prod_{j=1}^m X_{i,j}$
1	X	0	0	0	0
2	X	X	0	0	0
3	X	X	X	X	$X_3^* = \pm 1$
4	X	X	X	X	$X_4^* = \pm 1$
5	X	X	X	X	$X_5^* = \pm 1$
					$\tilde{M}_R^X = \text{Majority} \{X_i^*\}_{i=3,4,5}$ $= \text{sign} [\sum_{i=1}^n X_i^*]$

TABLE II: For (5,4)-QPC, the measurement strategy of \tilde{X} based on majority voting among $\{X_i^*\}_{i=3,\dots,5}$.

correction procedure for photon losses is similar. We use only the complete sub-blocks to determine the outcome of the encoded X measurements. In order to have successful recovery of quantum information encoded in the (n, m) -QPC, both of the following two conditions should be satisfied:

1. At least one qubit must arrive for each sub-block,
2. At least one sub-block must arrive with no loss.

Similarly, the encoded Z measurement can be performed in the presence of photon loss errors as illustrated in Table. III. The logical Z operator is given by, $\tilde{Z} \equiv \prod_{i=1}^n Z_{i,j}$ for $j = 1, \dots, m$. In the presence of photon loss errors, we may infer the encoded logical \tilde{Z} operator by $\prod_{i=1}^n Z_i^*$, where Z_i^* is obtained by majority voting from the i -th sub-block, as shown in Table. III. We use the majority voting scheme described above to perform error correction in the presence of both X and Z errors. We obtain analytic expressions for the success probability of error correction and the QBER of the protocol in the later sections.

IMPLEMENTATION OF TEC

In this section, we consider the implementation of TEC using cavity QED systems. Due to the fact that the encoded CNOT gate has a transversal implementation for CSS codes, we consider using cavity QED systems

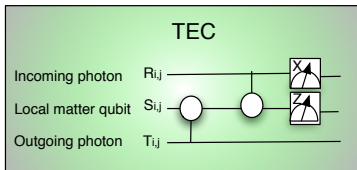


FIG. 5: (color online). The TEC quantum circuit at the level of physical qubits.

$i \setminus j$	1	2	3	4	$Z_i^* = \text{sign} [\sum_{j=1}^m Z_{i,j}]$
1	Z	0	0	0	$Z_1^* = \pm 1$
2	Z	Z	0	0	$Z_2^* = \pm 1$
3	Z	Z	Z	Z	$Z_3^* = \pm 1$
4	Z	Z	Z	Z	$Z_4^* = \pm 1$
5	Z	Z	Z	Z	$Z_5^* = \pm 1$
					$\tilde{M}_Z^S = \prod_{i=1}^n Z_i^*$

TABLE III: For (5,4)-QPC, measurement strategy of \tilde{Z} based on Z_i^* with $i = 1, \dots, n$.

to implement coupling gates between the local matter qubits and the incoming/outgoing photons.

The circuit at the encoded level (Fig.1(b) in the Letter) is very similar to the TEC circuit at the physical level (Fig. 5), consisting of Bell state preparation and Bell measurement. However, the determination of the Pauli frame is not based on the Bell measurement at physical level, but depending on the Bell measurement outcomes at encoded level. As shown in Fig. 5, we need to perform quantum gates that couple the incoming photon $R_{i,j}$, local qubits $S_{i,j}$, and outgoing photon $T_{i,j}$. After that, we measure the incoming photon $R_{i,j}$ in X basis and the local atom $S_{i,j}$ in Z basis.

To achieve a CNOT gate we may use the approach proposed by Duan and Kimble [1]. The CNOT gate can be reduced to two Hadamard gates and a CPHASE gate $CNOT_{a,b} = H_b \cdot CPHASE_{a,b} \cdot H_b$, with an efficiently implementation using cavity QED systems [1]. For example, with polarization encoding $\{H, V\}$ for the photon, a CPHASE gate can be achieved through an optical setup shown in Fig. 6. Using the implementation for a CPHASE gate shown in Fig. 6, the TEC circuit can be effectively implemented for an atom inside a cavity as shown in Fig. 7.

ERROR MODEL & PROBABILITY DISTRIBUTIONS

We consider both photon loss errors and operational error (due to imperfect gates and measurement). We

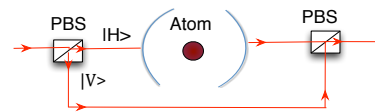


FIG. 6: (color online). Implementation of a CPHASE gate between a photon and an atom. The polarizing beam splitter (PBS) splits the path of the input photon depending on its polarization and the atom interacts with only photons with a certain polarization.

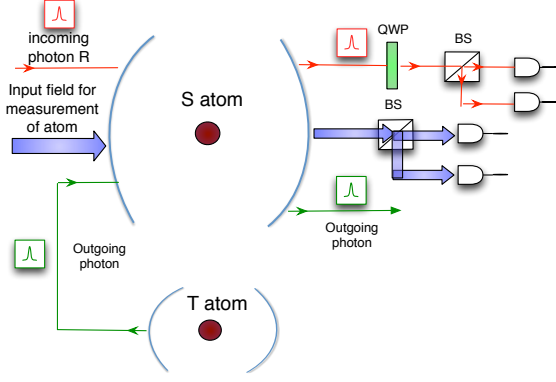


FIG. 7: (color online). A schematic view of the implementation of the TEC protocol between a single atom and a single photon. There two high Finesse cavities with S atom and T atom and the outgoing photon from the cavity containing the T atom enters the cavity containing S atom. In addition, the the incoming photon from the previous repeater station and the input field to control and measure the atom in the cavity enters the cavity. At the output, an additional quarter wave plate (QWP) is added for the X measurement of the incoming photon. The Z measurement is carried out by taking the photon through a beam splitter (BS) and detection.

assume that the qubits from the two encoded blocks (R and S) have independent errors before we perform the Bell measurement. Before the application of the CNOT gate, the combined state of R and S can be written as $\rho_{RS} = \rho_R \otimes \rho_S$. In the absence of CNOT gate errors, the application of a CNOT gate operation (denoted by U) on the state ρ_{RS} is given by $U\rho_{RS}U^\dagger$. In the presence of gate errors ϵ_g , the action of a noisy CNOT gate can be denoted with the super-operator

$$\mathcal{E}_{RS}(\rho_{RS}) = (1 - \epsilon_g)U\rho_{RS}U^\dagger + \frac{\epsilon_g}{16} \sum_{k=0}^3 \sum_{k=0}^3 \sigma_k^{(R)} \sigma_k^{(S)} \rho \sigma_k^{(R)} \sigma_k^{(S)}. \quad (6)$$

For qubit $R_{i,j}$, the error channel can be characterized by the following super-operator:

$$\rho'_R = \mathcal{E}_R(\rho_{RS}) = \eta(1 - \epsilon_d)\rho_R + \frac{\eta\epsilon_d}{4} \sum_{k=0}^3 \sigma_k \rho \sigma_k + (1 - \eta)|\text{vac}\rangle\langle\text{vac}|, \quad (7)$$

where $\eta = (1 - p_c)e^{-L_0/L_{att}}$ is the transmission probability, $1 - \eta$ is the photon loss error probability, ϵ_d is the probability of depolarization error for a transmitted qubit, ϵ is the effective qubit error which takes into account- measurement error ϵ_m and the gate error ϵ_g respectively and $\{\sigma_k\}_{k=0,\dots,3} = \{I, X, Y, Z\}$ are Pauli matrices including identity. Similarly, for the qubit $S_{i,j}$, the error channel can be characterized as

$$\rho'_S = \mathcal{E}_S(\rho_{RS}) = (1 - \epsilon_d)\rho_S + \frac{\epsilon_d}{4} \sum_{k=0}^3 \sigma_k \rho \sigma_k, \quad (8)$$

which only has depolarization error but no photon loss error because the S block consists of local qubits with no transmission loss. After the encoded Bell measurement (with transversal CNOT gates), the errors of the two encoding blocks become correlated. Hence, the measurement outcomes will become correlated between the two blocks, in particular the measurement outcome of the qubit pair $(R_{i,j}, S_{i,j})$ will become correlated. For example, a $Y_R X_S$ error will also induce a correlated error $Y_R X_S$ on the qubit pair $(R_{i,j}, S_{i,j})$. In order to compute the full distribution for the measurement outcome at the encoded level, we take the following three steps:

1. At the physical qubit level, we consider the errors associated with the qubit-pair measurement $(X_{i,j}^R, Z_{i,j}^S)$ for $i = 1, \dots, n$ and $j = 1, \dots, m$.
2. At the intermediate encoded level, we consider the errors associated with the row-pair measurement (X_i^{*R}, Z_i^{*S}) for $i = 1, \dots, n$.
3. At the logical encoded level, we consider the errors associated with the encoded-pair measurement $(\tilde{X}^R, \tilde{Z}^S)$.

In the following, we will compute three error probability distributions associated with these three different levels.

Probability distribution for qubit-pair measurement

First, we consider probability distribution associated with the qubit-pair measurement $(X_{i,j}^R, Z_{i,j}^S)$. For the ideal case with no loss or operational errors, we will have outcomes $(X_{i,j}^R, Z_{i,j}^S) = (r_{i,j}, s_{i,j})$ with $r_{i,j}, s_{i,j} = \pm 1$, but in the presence of errors the outcome will be $(X_{i,j}^R, Z_{i,j}^S) = (\alpha r_{i,j}, \beta s_{i,j})$ with $(\alpha, \beta) = (0, 0), (\pm 1, \pm 1), (\pm 1, \mp 1)$, which corresponds to the following cases:

1. $(\alpha, \beta) = (0, 0)$: Erasure error on $R_{i,j}$ with probability $\epsilon_e = \Pr[X_{i,j}^R = 0, Z_{i,j}^S = 0] = 1 - \eta$.
 2. $(\alpha, \beta) = (+1, -1)$: Spin-flip error in outcomes $(r_{i,j}, -s_{i,j})$, with probability $\epsilon_X = \Pr[X_{i,j}^R = r_{i,j}, Z_{i,j}^S = -s_{i,j}] = \eta \left(\frac{1}{2}\epsilon_d + \frac{1}{4}\epsilon_g + \epsilon_m + O(\epsilon_{d,g,m}^2) \right) = \frac{1}{2}\eta\epsilon$, where the effective error probability ϵ is defined as
- $$\epsilon = \epsilon_d + \frac{1}{2}\epsilon_g + \frac{1}{2}\epsilon_m + O(\epsilon_{d,g,m}^2). \quad (9)$$
3. $(\alpha, \beta) = (-1, -1)$: Spin-&-Phase-flip errors in outcomes $(-r_{i,j}, -s_{i,j})$, with probability $\epsilon_Y = \Pr[X_{i,j}^R = -r_{i,j}, Z_{i,j}^S = -s_{i,j}] =$

$\eta\left(\frac{1}{2}\epsilon_d + \frac{1}{4}\epsilon_g + O(\epsilon_{d,g,m}^2)\right) \lesssim \frac{1}{2}\eta\epsilon$, where the last step upper bounds the probability of the case of $(\alpha, \beta) = (-1, -1)$.

4. $(\alpha, \beta) = (-1, +1)$: Phase-flip error in outcomes $(-r_{i,j}, +s_{i,j})$, with probability $\epsilon_Z = \Pr[X_{i,j}^R = -r_{i,j}, Z_{i,j}^S = s_{i,j}] = \eta\left(\frac{1}{2}\epsilon_d + \frac{1}{4}\epsilon_g + \epsilon_m + O(\epsilon_{d,g,m}^2)\right) = \frac{1}{2}\eta\epsilon$.
5. $(\alpha, \beta) = (+1, +1)$: No change in the measurement outcomes of $(r_{i,j}, s_{i,j})$, with probability $\epsilon_I = \Pr[X_{i,j}^R = r_{i,j}, Z_{i,j}^S = s_{i,j}] = \eta\left(1 - \frac{3}{2}\epsilon_d - \frac{3}{4}\epsilon_g - 2\epsilon_m - O(\epsilon_{d,g,m}^2)\right) \gtrsim \eta(1 - \frac{3}{2}\epsilon)$.

Note $\epsilon_Y \neq (\epsilon_X + \epsilon_Y)(\epsilon_Z + \epsilon_Y)$ characterizing correlated errors. The sum of these probabilities is unity, $\epsilon_e + \epsilon_I + \epsilon_X + \epsilon_Y + \epsilon_Z = 1$.

Probability distribution for row-pair measurement

We now consider the distribution associated with the row-pair measurement (X_i^{*R}, Z_i^{*S}) . Suppose the ideal case, we will have outcomes $(X_i^{*R}, Z_i^{*S}) = (r_i, s_i)$ with $r_i, s_i = 0, \pm 1$, but in the presence of errors the outcome will be $(X_i^{*R}, Z_i^{*S}) = (\alpha r_i, \beta s_i)$ with $(\alpha, \beta) = (0, \pm 1) \otimes (0, \pm 1)$, with the following distribution:

$$q_{\alpha,\beta} := \Pr[X_i^* = \alpha r_i, Z_i^* = \beta s_i]. \quad (10)$$

Note that $q_{\alpha,\beta}$ does not depend on the row index i , because all rows have the same probability distribution.

In the measurement associated with the row-pair measurement, we may sum over all possible error patterns of qubit-pair measurement, with a photon loss errors (ϵ_e), b spin-flip errors (ϵ_X), c spin-&-phase-flip errors (ϵ_Y), d phase-flip errors (ϵ_Z), and $e = m - a - b - c - d$ faithful measurements (ϵ_I).

Because $X_i^{*R} = \prod_{j=1}^m X_{i,j}^R$ and $Z_i^{*S} = \text{sign}\left[\sum_{j=1}^n Z_{i,j}\right]$, the conditions are

$$\alpha = \begin{cases} 0 & \text{if } a \geq 1 \\ +1 & \text{if } a = 0 \text{ \& } (c+d) \text{ even} \\ -1 & \text{if } a = 0 \text{ \& } (c+d) \text{ odd} \end{cases} \quad (11)$$

and

$$\beta = \begin{cases} 0 & \text{if } 2(b+c) = m-a \\ +1 & \text{if } 2(b+c) < m-a \\ -1 & \text{if } 2(b+c) > m-a \end{cases}. \quad (12)$$

Then we can compute all $\{q_{\alpha,\beta}\}$. For example,

$$q_{0,0}$$

$$\begin{aligned} &= \sum_{a,b,c,d} \delta_{a \geq 1} \delta_{2(b+c)=m-a} \binom{m}{a,b,c,d} \epsilon_e^a \epsilon_X^b \epsilon_Y^c \epsilon_Z^d \epsilon_I^{m-a-b-c-d} \\ &= \sum_{a=1}^m \sum_{2w=m-a} \binom{m}{a,w} \epsilon_e^a (\epsilon_X + \epsilon_Y)^w (\epsilon_Z + \epsilon_I)^{m-a-w} \end{aligned}$$

with

$$\delta_{\text{cond}} := \begin{cases} 1 & \text{if cond = true} \\ 0 & \text{if cond = false} \end{cases}$$

and multinomial

$$\begin{aligned} &\binom{m}{a,b,c,d} \\ &= \binom{m}{a} \binom{m-a}{b} \binom{m-a-b}{c} \binom{m-a-b-c}{d}. \end{aligned}$$

Similarly we can compute the remaining $q_{\alpha,\beta}$:

$$q_{0,+1} = \sum_{a=1}^m \sum_{2w < m-a} \binom{m}{a,w} \epsilon_e^a (\epsilon_X + \epsilon_Y)^w (\epsilon_Z + \epsilon_I)^{m-a-w}$$

$$q_{0,-1} = \sum_{a=1}^m \sum_{2w > m-a} \binom{m}{a,w} \epsilon_e^a (\epsilon_X + \epsilon_Y)^w (\epsilon_Z + \epsilon_I)^{m-a-w}.$$

For the case with no photon losses, we have

$$\begin{aligned} q_{+1,0} &= \sum_{b,c,d} \delta_{(c+d)\text{even}} \delta_{2(b+c)=m} \binom{m}{b,c,d} \epsilon_X^b \epsilon_Y^c \epsilon_Z^d \epsilon_I^{m-b-c-d} \\ &= \sum_{v \text{ even}} \sum_{c=0}^v \sum_{b=\frac{m}{2}-c} \binom{m}{v-c,c,b} \epsilon_X^b \epsilon_Y^c \epsilon_Z^{v-c} \epsilon_I^{m-b-v} \end{aligned}$$

$$q_{+1,+1} = \sum_{v \text{ even}} \sum_{c=0}^v \sum_{b < \frac{m}{2}-c} \binom{m}{v-c,c,b} \epsilon_X^b \epsilon_Y^c \epsilon_Z^{v-c} \epsilon_I^{m-b-v}$$

$$q_{+1,-1} = \sum_{v \text{ even}} \sum_{c=0}^v \sum_{b > \frac{m}{2}-c} \binom{m}{v-c,c,b} \epsilon_X^b \epsilon_Y^c \epsilon_Z^{v-c} \epsilon_I^{m-b-v},$$

and

$$q_{-1,0} = \sum_{v \text{ odd}} \sum_{c=0}^v \sum_{b=\frac{m}{2}-c} \binom{m}{v-c,c,b} \epsilon_X^b \epsilon_Y^c \epsilon_Z^{v-c} \epsilon_I^{m-b-v}$$

$$q_{-1,+1} = \sum_{v \text{ odd}} \sum_{c=0}^v \sum_{b < \frac{m}{2}-c} \binom{m}{v-c,c,b} \epsilon_X^b \epsilon_Y^c \epsilon_Z^{v-c} \epsilon_I^{m-b-v}$$

$$q_{-1,-1} = \sum_{v \text{ odd}} \sum_{c=0}^v \sum_{b > \frac{m}{2}-c} \binom{m}{v-c,c,b} \epsilon_X^b \epsilon_Y^c \epsilon_Z^{v-c} \epsilon_I^{m-b-v}.$$

Probability distribution for encoded-pair measurement

We now consider the distribution associated with the encoded-pair measurement (\tilde{X}, \tilde{Z}) . For the ideal case, we will have outcomes $(\tilde{M}_X^R, \tilde{M}_Z^S) = (\tilde{X}^R, \tilde{Z}^S)$ with $\tilde{X}^R, \tilde{Z}^S = \pm 1$, but in the presence of errors the outcome will be $(\tilde{M}_X^R, \tilde{M}_Z^S) = (\alpha \tilde{X}^R, \beta \tilde{Z}^S)$ with $(\alpha, \beta) = (0, \pm 1) \otimes (0, \pm 1)$, with the following distribution:

$$p_{\alpha, \beta} := \Pr \left[\tilde{M}_X = \alpha \tilde{X}^R, \tilde{M}_Z = \beta \tilde{Z}^S \right]. \quad (13)$$

In the measurement associated with the encoded-pair measurement, we may sum over all possible error patterns of row-pair measurements, with a instances of $(q_{0,0})$, b instances of $(q_{1,0})$, c instances of $(q_{-1,0})$, d in-

stances $(q_{0,1})$, e instances of $(q_{1,1})$, f instances of $(q_{-1,1})$, g instances of $(q_{0,-1})$, h instances of $(q_{1,-1})$, i instances of $(q_{-1,-1})$, with $a + b + c + d + e + f + g + h + i = n$.

Because $\tilde{M}_X^R = \text{sign} \left[\sum_{i=1}^n X_i^* \right]$ and $\tilde{M}_Z^S = \prod_{i=1}^n Z_i^*$, then the conditions are

$$\tilde{M}_X^R = \begin{cases} 0 & \text{if } 2(b + e + h) = n - (a + d + g) \\ +1 & \text{if } 2(b + e + h) > n - (a + d + g) \\ -1 & \text{if } 2(b + e + h) < n - (a + d + g) \end{cases} \quad (14)$$

and

$$\tilde{M}_Z^S = \begin{cases} 0 & \text{if } a + b + c \geq 1 \\ +1 & \text{if } a + b + c = 0 \text{ \& } (g + h + i) \text{ even} \\ -1 & \text{if } a + b + c = 0 \text{ \& } (g + h + i) \text{ odd} \end{cases} \quad (15)$$

Finally, we can compute all $\{p_{\alpha, \beta}\}$:

$$\begin{aligned} p_{0,0} &= \sum_{a,b,c,d,e,f,g,h} \delta_{a+b+c \geq 1} \delta_{2(b+e+h)=n-(a+d+g)} \binom{n}{a,b,c,d,e,f,g,h} q_{0,0}^a q_{1,0}^b q_{-1,0}^c q_{0,1}^d q_{1,1}^e q_{-1,1}^f q_{0,-1}^g q_{1,-1}^h q_{-1,-1}^{n-(a+b+c+d+e+f+g+h)} \\ &= \sum_{a,b,c,v,w} \delta_{a+b+c \geq 1} \delta_{2(b+w)=n-a-v} \binom{n}{a,b,c,v,w} q_{0,0}^a q_{1,0}^b q_{-1,0}^c (q_{0,1} + q_{0,-1})^v (q_{1,1} + q_{-1,1})^w (q_{1,-1} + q_{-1,-1})^{n-(a+b+c+v+w)} \end{aligned}$$

$$p_{1,0} = \sum_{a,b,c,v,w} \delta_{a+b+c \geq 1} \delta_{2(b+w) > n-a-v} \binom{n}{a,b,c,v,w} q_{0,0}^a q_{1,0}^b q_{-1,0}^c (q_{0,1} + q_{0,-1})^v (q_{1,1} + q_{-1,1})^w (q_{1,-1} + q_{-1,-1})^{n-(a+b+c+v+w)}$$

$$p_{-1,0} = \sum_{a,b,c,v,w} \delta_{a+b+c \geq 1} \delta_{2(b+w) < n-a-v} \binom{n}{a,b,c,v,w} q_{0,0}^a q_{1,0}^b q_{-1,0}^c (q_{0,1} + q_{0,-1})^v (q_{1,1} + q_{-1,1})^w (q_{1,-1} + q_{-1,-1})^{n-(a+b+c+v+w)}$$

$$p_{0,1} = \sum_{d,e,g,h,i} \delta_{(g+h+i) \text{ even}} \delta_{2(e+h)=n-d-g} \binom{n}{d,e,g,h,i} q_{0,1}^d q_{1,1}^e q_{-1,1}^{n-(d+e+g+h+i)} q_{0,-1}^g q_{1,-1}^h q_{-1,-1}^i$$

$$p_{1,1} = \sum_{d,e,g,h,i} \delta_{(g+h+i) \text{ even}} \delta_{2(e+h) > n-d-g} \binom{n}{d,e,g,h,i} q_{0,1}^d q_{1,1}^e q_{-1,1}^{n-(d+e+g+h+i)} q_{0,-1}^g q_{1,-1}^h q_{-1,-1}^i$$

$$p_{-1,1} = \sum_{d,e,g,h,i} \delta_{(g+h+i) \text{ even}} \delta_{2(e+h) < n-d-g} \binom{n}{d,e,g,h,i} q_{0,1}^d q_{1,1}^e q_{-1,1}^{n-(d+e+g+h+i)} q_{0,-1}^g q_{1,-1}^h q_{-1,-1}^i$$

$$p_{0,-1} = \sum_{d,e,g,h,i} \delta_{(g+h+i) \text{ odd}} \delta_{2(e+h)=n-d-g} \binom{n}{d,e,g,h,i} q_{0,1}^d q_{1,1}^e q_{-1,1}^{n-(d+e+g+h+i)} q_{0,-1}^g q_{1,-1}^h q_{-1,-1}^i$$

$$p_{1,-1} = \sum_{d,e,g,h,i} \delta_{(g+h+i) \text{ odd}} \delta_{2(e+h) > n-d-g} \binom{n}{d,e,g,h,i} q_{0,1}^d q_{1,1}^e q_{-1,1}^{n-(d+e+g+h+i)} q_{0,-1}^g q_{1,-1}^h q_{-1,-1}^i$$

$$p_{-1,-1} = \sum_{d,e,g,h,i} \delta_{(g+h+i) \text{ odd}} \delta_{2(e+h) < n-d-g} \binom{n}{d,e,g,h,i} q_{0,1}^d q_{1,1}^e q_{-1,1}^{n-(d+e+g+h+i)} q_{0,-1}^g q_{1,-1}^h q_{-1,-1}^i.$$

FAULT-TOLERANT PREPARATION OF THE ENCODED BELL PAIR

In this section, we will provide key procedures to prepare an encoded Bell state at every repeater station for the teleportation based fault-tolerant quantum error correction. We assume that there are long range interconnects for state preparation, making the physical location of the qubits irrelevant. For example, this can be achieved in an anharmonic linear ion trap [2].

We can use stabilizer notations to define the (n, m) -QPC. First, we define the Pauli operators, $X_{i,j}, Y_{i,j}, Z_{i,j}$ for the (i, j) -th qubit, where $i = 1, \dots, n$ is the row (sub-block) label and $j = 1, \dots, m$ is the column label for the qubit. The stabilizers [3] for the (n, m) -QPC can be defined by the following

$$S_{i,j} \equiv Z_{i,j} Z_{i,j+1}$$

for $i = 1, \dots, n$ and $j = 1, \dots, m-1$, and

$$S_{i,0} \equiv \prod_{j=1}^m X_{i,j} X_{i+1,j}$$

for $i = 1, \dots, n-1$. Given the above $nm-1$ independent stabilizers, there is one logical qubit encoded in the (n, m) -QPC, with logical operators

$$\tilde{Z} \equiv \prod_{i=1}^n Z_{i,1} = \prod_{i=1}^n Z_{i,2} = \dots = \prod_{i=1}^n Z_{i,m}$$

$$\tilde{X} \equiv \prod_{j=1}^m X_{1,j} = \prod_{j=1}^m X_{2,j} = \dots = \prod_{j=1}^m X_{n,j}.$$

The distance of the code is given by $d = \min(n, m)$.

In order to create the encoded Bell pair, we need to create the encoded states $|0\rangle_L$ and $|+\rangle_L$ fault-tolerantly, and then apply transversal CNOT gate to obtain the encoded Bell pair $|\psi^{ab}\rangle_L = \frac{1}{\sqrt{2}}(|00\rangle_L + |11\rangle_L)$. (1) The state $|+\rangle_L = \frac{1}{2^{n/2}}(|00\dots 0\rangle_{12\dots m} + |11\dots 1\rangle_{12\dots m})^{\otimes n}$ is easy to prepare because it is a product of several GHZ states, which can be obtained fault-tolerantly by repetitive check of weight-two stabilizers $Z_{i,j} Z_{i,j+1}$. (2) The state $|0\rangle_L$ can also be prepared fault-tolerantly: First, we initialize all physical qubits in the $|0\rangle$ state, which ensures that we have $S_{i,j} = 1$ and $\tilde{Z} = 0$. Then, we repeatedly measure the stabilizers $S_{i,0}$ with GHZ states that are also prepared fault-tolerantly, and obtain the final state $|0'\rangle_L$. We define the modified stabilizers $S'_{i,0} = K_{i,0} S_{i,0} = 1$,

with $K_{i,0} = \pm 1$ depending on the measurement outcome of $S_{i,0}$. The value of $K_{i,0}$ can be obtained by the majority vote of many repetitive and fault-tolerant measurements to suppress any potentially correlated error to a sufficiently high order. We will use $|0'\rangle_L$, which is equivalent to $|0\rangle_L$ up to a sign change of $S_{i,0}$. It is easy to check that $S_{i,0}|0'\rangle_L = K_{i,0}|0'\rangle_L$. (3) Any sign change associated with $K_{i,0}$ can be easily updated for all later operations of transversal CNOT gates and X or Z measurements. For example, the encoded Bell pair $|\psi^{ab}\rangle_L = \frac{1}{\sqrt{2}}(|00\rangle_L + |11\rangle_L)$ can be prepared by applying a transversal CNOT gate between $|\phi^a\rangle = |+\rangle_L$ and $|\phi^b\rangle = |0'\rangle_L$. The encoded Bell state $|\psi^{ab}\rangle_L$ has stabilizers $\tilde{X}^a \tilde{X}^b, \tilde{Z}^a \tilde{Z}^b, S_{i,j}^a, S_{i,j}^b$ and $S_{i,0}^a |\psi^{ab}\rangle_L = S_{i,0}^b |\psi^{ab}\rangle_L = K_{i,0} |\psi^{ab}\rangle_L$.

ERROR ANALYSIS FOR STATE PREPARATION

We now detail the calculation for the procedure for the fault tolerant encoded Bell state preparation in three steps:

First, we can prepare physical Bell pairs $|\psi_{\pm}\rangle = \frac{1}{\sqrt{2}}(|00\rangle + |11\rangle)$ with a high fidelity by employing entanglement purification techniques (locally). In the presence of gate errors, we obtain the state $\rho = (1 - \epsilon_g)|\psi_{\pm}\rangle\langle\psi_{\pm}| + \epsilon_g \frac{I}{4}$, which is only limited by the gate error probability ϵ_g . Then we use entanglement purification to suppress the bit-flip errors in the Bell state by preparing l copies of the Bell state and measuring the error syndromes as shown in Fig. 8. After the purification process and elimination, the state is now given by,

$$\rho_p = (1 - l \cdot \epsilon_g - \epsilon_g^l - l \cdot \epsilon_g^{(l+1)}) |\psi_{\pm}\rangle\langle\psi_{\pm}| + l \cdot \epsilon_g |\psi_{-}\rangle\langle\psi_{-}| + \epsilon_g^l |\phi_{\pm}\rangle\langle\phi_{\pm}| + l \cdot \epsilon_g^{(l+1)} |\phi_{-}\rangle\langle\phi_{-}|$$

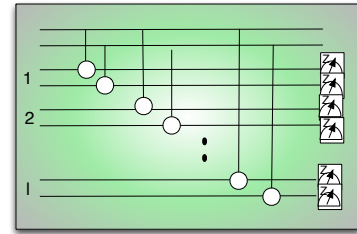


FIG. 8: (color online). 1, 2, 3, ... l are in the state $|\psi_{\pm}\rangle$. Repetitive measurement is carried out for the suppression of bit-flip errors in the creation of a Bell pair.

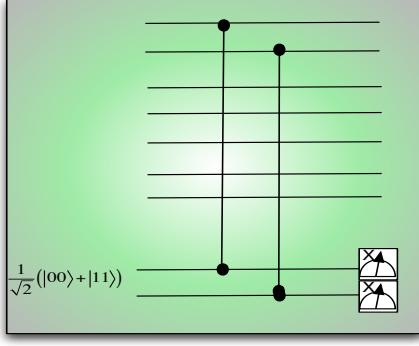


FIG. 9: (color online). The syndrome of $Z_{i,j}Z_{i,j+1}$ is measured repetitively $2k + 1$ times. Controlled-Phase gates don't propagate bit-flip errors

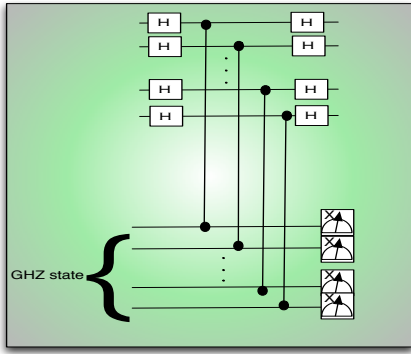


FIG. 10: (color online). The fault tolerant preparation of the CSS code using syndrome measurement using a GHZ state. The syndrome is repeated $2h + 1$ times.

For $l > 1$, and $\epsilon_g \ll 1$ this is given by,

$$\rho_p \approx (1 - l \cdot \epsilon_g)|\psi_+\rangle\langle\psi_+| + l \cdot \epsilon_g|\psi_-\rangle\langle\psi_-|.$$

Second, we use these Bell pairs with suppressed bit flip errors for the fault tolerant preparation of GHZ states by using repetitive measurements for the extraction the syndrome measurement $Z_{i,j}Z_{i,j+1}$ as shown in the Fig. 9. Note that the dephasing of a Bell state induces an error syndrome in the X-measurement and a bit-flip error in a Bell state induces the dephasing of a qubit in the GHZ state. The probability of having an error syndrome and the probability of dephasing of a qubit in the r -qubit GHZ state are given by,

$$p_{GHZ,syndrome} = \sum_{j=k}^r \left[\binom{r}{j} (l \cdot \epsilon_g)^j (1 - l \cdot \epsilon_g)^{(r-j)} \right]$$

$$p_{GHZ,dephasing} \leq [1 - (1 - \epsilon_g)^{(2k+1)} + \epsilon_g].$$

We use m -qubit GHZ state for the fault-tolerant preparation of $|+\rangle_L$ state. In addition, we use $2m$ -qubit GHZ state for the stabilizer measurements of $|0\rangle_L$ state, as shown in Fig. 10.

Finally, the effective measurement error for the CSS code for one round of measurement is given by,

$$\epsilon_z = \epsilon_m + \epsilon_g + \tilde{p}_{GHZ,dephasing} + \tilde{p}_{GHZ,syndrome}, \quad (17)$$

where ϵ_m and ϵ_g are the measurement errors and gate errors respectively. Since, odd number of dephasing errors only contribute to the dephasing of the GHZ state, we have the effective phase error p_{phase} of the CSS code as

$$p_{phase} = \sum_{r=1,3,\dots}^{2m} \binom{2m}{r} \epsilon_z^r (1 - \epsilon_z)^{2m-r}. \quad (18)$$

We then perform a majority voting of the measurement outcomes. So, the probability that there is a syndrome error and dephasing errors in the CSS code are given by,

$$p_{CSS,syndrome} = \sum_{j=h}^{2m} \left[\binom{2m}{j} p_{phase}^j (1 - p_{phase})^{(2m-j)} \right].$$

$$p_{CSS,dephasing} = \epsilon_g + \tilde{p}_{GHZ,syndrome}$$

Similarly, we apply n different syndrome measurements for every consecutive pair of rows. For QPC

$$p_{QPC,syndrome} = (p_{CSS,syndrome})^n$$

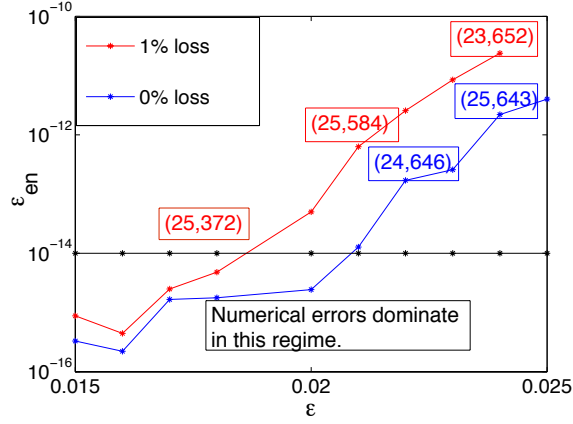
$$p_{QPC,dephasing} = 2 \times p_{CSS,dephasing}. \quad (19)$$

It can be verified that $\tilde{p}_{GHZ,syndrome} \ll \epsilon_g$ by multiple measurements leading to $p_{CSS,dephasing} \approx \epsilon_g$. To get an estimate of this calculation, for gate errors $\epsilon_g = 0.007$, $m = 6$, $n = 14$, $\epsilon_m = 10^{-4}$ and choosing $h = k = l = 5$, we can achieve $p_{QPC,syndrome} \approx 0$ and $p_{QPC,dephasing} = \epsilon_g \approx 0.014$.

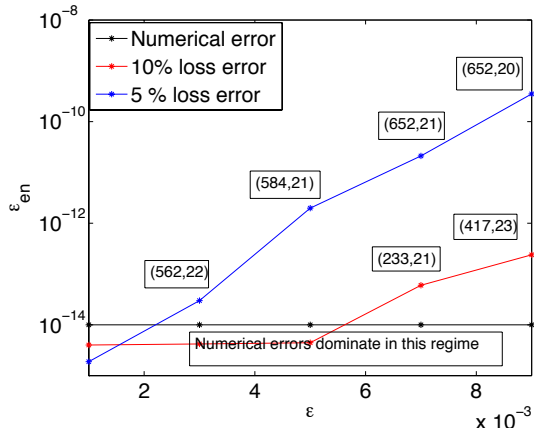
FAULT TOLERANT PROPERTIES OF QPC

An important difference between fault tolerant quantum computers and fault tolerant quantum repeaters is that loss errors play an important role in the latter. For a single transmission of QPC between neighboring QR stations, we can define the effective encoded error rate to be $\epsilon_{en} = (1 - p_{1,1})$, which takes into account both heralded failure and quantum bit error rates. Analogous to a recent study on Bacon-Shor codes [4], we show in Fig. 11 that it is possible to suppress the encoded error to $\epsilon_{en} \approx 10^{-14}$ by choosing an appropriate encoding with a large number of qubits in a specific range for ϵ , (a) $1.5 \times 10^{-2} \leq \epsilon \leq 2.5 \times 10^{-2}$ in the absence of loss errors and in the presence of low loss errors (1%). (b) $1 \times 10^{-3} \leq \epsilon \leq 9 \times 10^{-3}$ in the presence of higher loss errors (5%, 10%).

Alternatively, we confirm with numerical calculations that in the absence of loss errors and in the presence of loss errors (up to (10%)), it is possible to arbitrarily suppress the encoded error rate - which accounts for both the bit-error rate and the failure probabilities to $\epsilon_{en} \approx 10^{-14}$. Below 10^{-14} , numerical errors begin to play an important role. The results are summarized in the Table IV.



(a)



(b)

FIG. 11: (color online). Optimum logical error rate ϵ_{en} vs physical error rate ϵ (a) for no losses and 1% loss errors. (b) for 5% loss errors and 10% loss errors. Numerical errors begin to dominate in the range $\epsilon_{en} \approx 10^{-14}$.

$\epsilon \backslash p_c(1-\eta)$	0%	1%	5%	10%
10^{-3}	(13,9)	(28,14)	(112,20)	(372,21)
6×10^{-4}	(17,11)	(25,12)	(154,16)	(235,19)
3×10^{-4}	(13,11)	(20,12)	(54,14)	(230,19)
10^{-4}	(11,9)	(17,10)	(49,13)	(221,19)

TABLE IV: QPC codes that are required to achieve an encoded error rate of $\epsilon_{en} \approx 10^{-14}$ for different physical error rates ϵ in the presence of varying losses in %.

DETAILS OF THE OPTIMIZATION ALGORITHM

A self explanatory flow chart of the optimization algorithm used in the Letter for the minimal cost coefficient of third class of QRs is shown in Fig. 12. We start the search with $L_{tot} = 500$ km, $L_0 = 1$ km and $m = n = 2$.

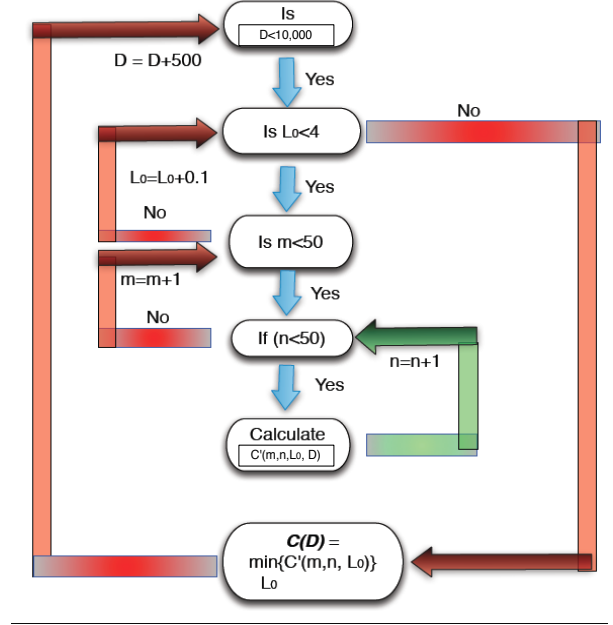


FIG. 12: (color online). The flow chart of the algorithm to find the optimized QR parameters. The units of L_{tot} and L_0 are in km and are ignored in the figure for convenience.

SCALING OF THE COST COEFFICIENT

In the absence of a QR, the cost coefficient scales exponentially with the distance across which the communication is desired. In the presence of our QRs, a numerical investigation (Fig. 13) of the cost coefficient indicates that it has a poly-logarithmic scaling with the total distance of communication up to $L_{tot} = 10^4$ km in the absence and in the presence of coupling losses (up to $p_c = 10\%$), respectively. In the regime where ϵ is smaller than 10^{-3} and there are no coupling losses, the QBER and the success probability are dominated by the photon loss errors and the cost coefficient scales as $\approx O(\log D)^2$. As the contribution of ϵ to the final success probability and QBER increases, the quadratic scaling breaks, but the scaling of the cost coefficient still seems to be poly-logarithmic with distance.

GENERALIZED COST COEFFICIENT

The cost coefficient introduced in the letter is defined for the case when the cost of the qubits are expensive, but it is possible to envision a scenario, where qubits may be cheap. Taking this into account, we can define the *generalized cost coefficient* to be

$$C' = \frac{(2nm)^k}{R \cdot L_0}, \quad (20)$$

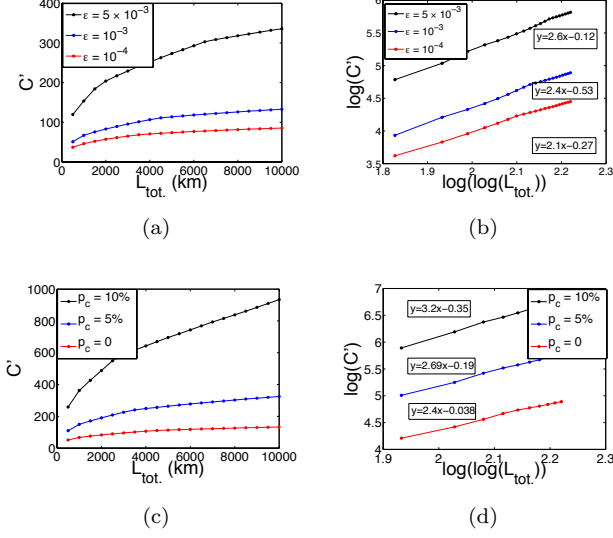


FIG. 13: (color online). (a) $C'(L_{tot})$ for various ϵ 's up to 10^4 km, (b) Indication of poly-logarithmic scaling of (a), (c) $C'(L_{tot})$ for $\epsilon = 10^{-3}$ up to 10^4 km with coupling losses, (d) Indication of poly-logarithmic scaling of (c). We assume $t_0 = 1$ in (a), (b), (c) and (d) for convenience.

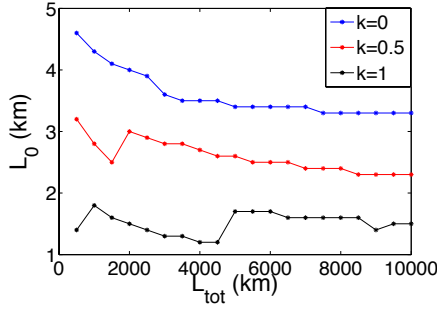


FIG. 14: (color online). For a range of search $2 \leq (n, m) \leq 50$, $\epsilon = 10^{-3}$ and $p_c = 0$, Optimal repeater spacing for various k 's. Note that for $k = 0$, it is possible to have a larger repeater spacing by increasing the range of search.

where k is a constant satisfying $0 \leq k \leq 1$. The choice of the above definition is guided by the constraint to obtain a unitless cost coefficient which scales polynomial in the number of qubits. For $k = 0$, qubits cost absolutely nothing and $k = 1$ corresponds to the case considered in the letter, which takes into account the cost of the qubits. A comparison of the cost coefficients for different k 's is shown in Fig. 14.

Interestingly, it is possible to have higher repeater spacings for the case where the qubits are cheap as shown in Fig. 14. For $k = 0$, one can have a higher repeater spacing by increasing the range of search. To provide an estimate, for $\epsilon = 10^{-3}$ and $p_c = 0$, to generate a secret key across 1000 km, with 800 qubits per repeater station, one can have a repeater spacing of 4.3 km and with 8500 qubits per repeater station, one can have a repeater spacing of 6.3 km. Similarly, to generate a secret key across 10,000 km, with 1000 qubits per repeater station, one can have a repeater spacing of 4.1 km and with 9100 qubits per repeater station, one can have a repeater spacing of 5.5 km.

-
- [1] L. M. Duan and H. J. Kimble, Phys. Rev. Lett. **92**, 127902 (2004).
 - [2] G.-D. Lin, S.-L. Zhu, R. Islam, K. Kim, M.-S. Chang, S. Korenblit, C. Monroe and L.-M. Duan, EuroPhys. Lett. **86**, 60004 (2009).
 - [3] D. Gottesman, Caltech Ph.D. Thesis (1997).
 - [4] P. Brooks and J. Preskill, Phys. Rev. A **87**, 032310 (2013).